Journal of Structural Geology 32 (2010) 1656–1667

Contents lists available at ScienceDirect

Journal of Structural Geology

journal homepage: www.elsevier.com/locate/jsg

Normal-fault development during two phases of non-coaxial extension: An experimental study

Alissa A. Henza*, Martha O. Withjack, Roy W. Schlische

Department of Earth & Planetary Sciences, Rutgers University, 610 Taylor Road, Piscataway, NJ 08854-8066, USA

ARTICLE INFO

Article history:
Received 29 January 2009
Received in revised form
24 June 2009
Accepted 26 July 2009
Available online 4 August 2009

Keywords:
Normal faults
Experimental modeling
Multiple phases of extension
Fault reactivation

ABSTRACT

We use scaled experimental (analog) models to study the effect of a pre-existing fault fabric on fault development during extension. In our models, a homogeneous layer of wet clay undergoes two non-coaxial phases of extension whose directions differ by up to 45°. The normal faults that develop during the first phase create a pronounced fault fabric that influences normal-fault development during the second phase. In all models, the pre-existing faults are reactivated during the second phase of extension. Their sense of slip depends on the angle between the first- and second-phase extension directions. Specifically, the component of dip slip relative to strike slip decreases as the angle between the first- and second-phase extension directions increases. New normal faults also form during the second phase of extension in all models. The number of new fault segments increases as the angle between the first- and second-phase extension directions increases. The orientations of the new normal-fault segments are both orthogonal and oblique to the second-phase extension direction, indicating that both the second-phase extension direction and the pre-existing fault fabric control the orientation of new fault segments. Some of the new normal faults cut and offset the pre-existing faults, whereas others terminate against them, producing complex fault patterns and interactions. The modeling results explain fault interactions observed in the Jeanne d'Arc rift basin of offshore Newfoundland, Canada, and the reactivation of abyssal-hill normal faults at outer highs near subduction zones.

1. Introduction

Many extensional provinces have undergone more than one episode of deformation. For example, researchers have recognized multiple phases of non-coaxial extension in the Jeanne d'Arc rift basin (e.g., Enachescu, 1987; Tankard and Welsink, 1987; Sinclair, 1995a, b; Sinclair and Withjack, 2008), the North Sea (e.g., Badley et al., 1988; Bartholomew et al., 1993; Færseth, 1996), Thailand (e.g., Morley et al., 2004, 2007), and the East African rift system (e.g., Strecker et al., 1990). Although these studies provide valuable information about fault orientations and interactions in areas with complex extensional histories, several critical questions remain. How does the fault pattern that forms during an early episode of extension affect the fault patterns that form during subsequent episodes of extension? What factors determine whether faults are reactivated or new faults form during subsequent deformation? How do pre-existing normal faults affect the initiation, propagation, and geometry of newly formed normal faults? The goal of our research is to address these critical questions. Specifically, we use scaled experimental (analog) models to simulate two phases of non-coaxial extension and study how the angle between the extension directions affects the resultant deformation patterns. We also compare the modeling results with natural fault patterns in regions that have undergone multiple phases of extension.

2. Experimental approach

2.1. Modeling materials

Most scaled experimental models of extension use either dry sand or wet clay as the primary modeling material (e.g., Eisenstadt and Sims, 2005; Withjack et al., 2007, and references therein). Deformation patterns in sand and clay models of extension have similarities and differences (Withjack and Callaway, 2000; Eisenstadt and Sims, 2005; Withjack and Schlische, 2006; Withjack et al., 2007). In both sand and clay models, normal faults form that strike 90° to the extension direction. Fault-zone widths, however, are much greater in sand models (>1.0 mm) than in clay models (<0.1 mm). Also, most deformation is localized on a few major normal faults in sand models, whereas deformation is distributed

* Corresponding author. Tel.:+1 732 445 2125.
E-mail addresses: ahenza@rci.rutgers.edu (A.A. Henza), drmeow3@rci.rutgers.edu (M.O. Withjack), schlisch@rci.rutgers.edu (R.W. Schlische).

0191-8141/$ – see front matter © 2009 Elsevier Ltd. All rights reserved.
doi:10.1016/j.jsg.2009.07.007

among major normal faults, minor normal faults, and folds in clay models. In this study, we use wet clay as the modeling material to provide a more detailed view of fault interactions and evolution. The wet clay is similar to that used in other experimental modeling studies (e.g., Withjack and Callaway, 2000; Eisenstadt and Sims, 2005; Withjack and Schlische, 2006; Withjack et al., 2007). It is composed mainly of kaolinite particles (<0.005 mm in diameter) and water (~40% by weight) and has a density of 1.55–1.60 g cm^{-3}. Its coefficient of internal friction is ~0.6, and its cohesive strength is ~ 50 Pa.

To ensure dynamic similarity between the experimental models and natural prototypes, two conditions must be satisfied (e.g., Hubbert, 1937; Nalpas and Brun, 1993; Weijermars et al., 1993). First, the modeling material must have a similar coefficient of friction to that of rocks in nature. For most sedimentary rocks, the coefficient of friction ranges between 0.55 and 0.85 (e.g., Handin, 1966; Byerlee, 1978). Thus, the wet clay in our models (with a coefficient of friction of ~0.6) is a suitable modeling material. Second, the models must obey the scaling relationship:

$$C^* = \rho^* \times L^* \times g^* \quad (1)$$

where C^*, ρ^*, L^*, and g^* are the model to prototype ratios for cohesion, density, length, and gravity, respectively. In our models, the value of ρ^* is 0.7 and g^* is 1. Thus, C^* and L^* must have similar magnitudes to ensure dynamic similarity. In nature, C ranges from less than 1 MPa (for loosely compacted sedimentary rocks) to more than 10 MPa (for intact igneous or metamorphic rocks) (Handin, 1966; Schellart, 2000; and references therein). Additionally, C can be significantly less than 1 MPa for fractured rocks (e.g., Byerlee, 1978; Brace and Kohlstedt, 1980). As mentioned previously, the wet clay in our models has a cohesive strength of ~50 Pa, resulting in a value of C^* between 10^{-4} and 10^{-6}. Therefore, L^* ranges between 10^{-4} and 10^{-6} in our models, depending on the cohesion of the natural prototype. If the clay simulates a layer of loosely compacted sedimentary rock, then 1 cm in the model represents ~100 m in nature. Alternatively, if the clay simulates intact crystalline rock, then 1 cm in the model represents about ~10 km in nature.

2.2. Experimental set-up

Our experimental set-up resembles that in previous experimental models of oblique extension (e.g., Withjack and Jamison, 1986; Tron and Brun, 1991; McClay and White, 1995; Bonini et al., 1997; Keep and McClay, 1997; Clifton et al., 2000). The base of the apparatus consists of an 8-cm wide rubber sheet attached to two rigid sheets (one fixed and one mobile) (Fig. 1a). A 0.5-cm thick layer of silicone polymer, with a viscosity of ~10^4 Pa s (Weijermars, 1986), overlies the rubber sheet. A layer of wet clay covers the layer of silicone polymer, the fixed rigid sheet, and the mobile rigid sheet (Fig. 1b). It is 3.5 cm thick above the layer of silicone polymer and 4.0 cm thick above the rigid sheets. During the experiments, the mobile rigid sheet moves outward, stretching the attached rubber sheet and the overlying silicone polymer (Fig. 1a). In response, a deformation zone develops within the clay layer above the rubber sheet and silicone polymer. The silicone polymer serves two functions in our models: it localizes deformation within the clay layer above the rubber sheet (e.g., Bellahsen et al., 2003), and it decouples the clay layer from the rubber sheet (allowing the base of the clay layer to move vertically).

Based on Withjack and Jamison (1986), α is the clockwise angle measured from the trend of the deformation zone within the clay layer to the displacement direction of the mobile rigid sheet (Fig. 1a). Oblique deformation with both extensional and shear components results when $\alpha \neq 0°$, $\alpha \neq 90°$, or $\alpha \neq 180°$ (Withjack and Jamison, 1986). Furthermore, when $\alpha \neq 90°$, the maximum extension direction and displacement direction differ: the maximum extension direction lies midway between the displacement direction and the normal to the trend of the deformation zone (see Withjack and Jamison (1986) for details). Previous models of oblique extension (e.g., Withjack and Jamison, 1986; Tron and Brun, 1991; Clifton et al., 2000) have shown that only normal faults form when $45° \leq \alpha \leq 135°$ (Fig. 2a). For $\alpha < 45°$ and $\alpha > 135°$, normal, oblique-slip and/or strike-slip faults develop.

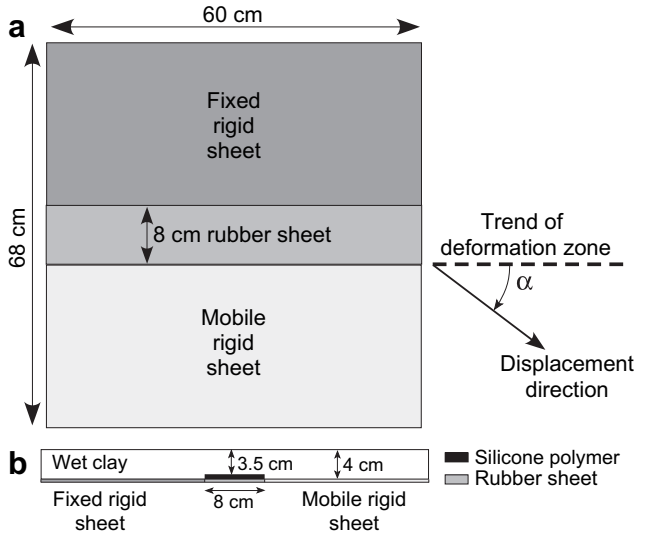

Fig. 1. Experimental set-up in (a) plan view and (b) cross section. Plan view set-up shows definition of α (based on Withjack and Jamison, 1986).

All models in this study have two phases of deformation (Fig. 2b). During the first phase, the mobile sheet moves outward at a rate of 4 cm h^{-1} (1.1 × 10^{-3} cm s^{-1}) in a prescribed direction ($\alpha_1 = 45°$) for a prescribed displacement (3.5 cm). In response, a pervasive (but not continuous) fabric consisting of normal faults develops throughout the deformation zone in the clay layer. During the second phase, the mobile plate moves outward at a rate of 4 cm h^{-1} in a different prescribed direction ($\alpha_2 = 135°$, 120°, 105°, or 90°; see Fig. 2b) for a prescribed distance (3.5 cm). Thus, the angle between the first- and second-phase *displacement* directions varies from 90° to 45° in our models (Figs. 1, 2), whereas the angle between the first- and second-phase *extension* directions varies from 45° to 22.5° (Fig. 2b).

2.3. Model analysis

Photographs of the top surface of the clay layer, taken at regular time intervals, record the surface deformation through time during both phases of extension. To exclude edge effects, we analyze only the central part of the top surface of the deformation zone. Offsets of superficial linear markers on the top surface of the clay layer indicate the sense of slip on faults during both phases of extension (Fig. 3a). We confirm the sense of slip by observing corrugations on the fault surfaces at the end of each experiment (Fig. 3b). Corrugations are grooves on fault surfaces that parallel the slip direction (Granger, 2006; Granger et al., 2006, Granger et al., 2008). To determine the numbers and orientations of fault segments, we fit straight lines to individual fault segments (Fig. 3c, d). Fitting lines to fault segments, rather than drawing lines from fault tip to fault tip, captures all segment orientations in areas where second-phase faults have linked with first-phase faults. To determine whether deformation patterns changed significantly with depth, we also examined the bottom surface of a dried model with boundary conditions identical to Model 1 ($\alpha_1 = 45°$ and $\alpha_2 = 135°$).

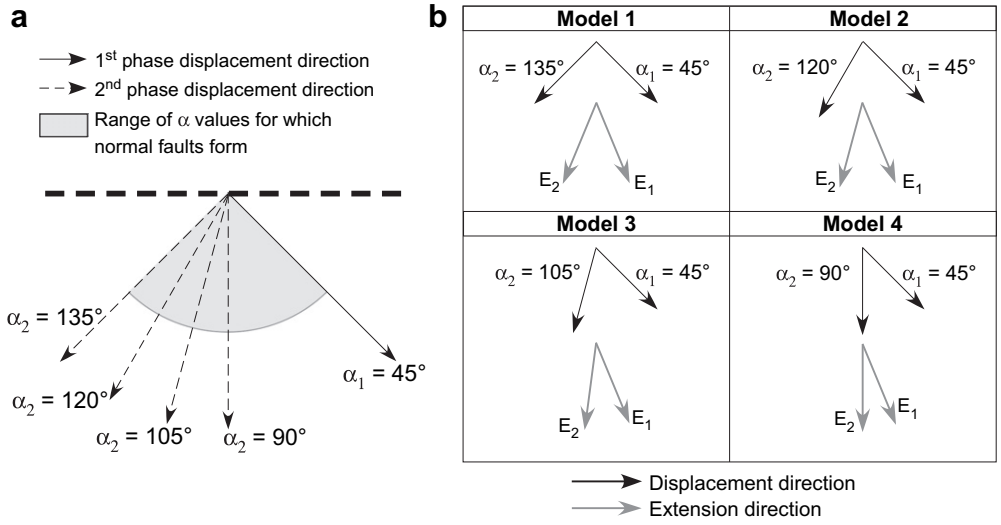

Fig. 2. (a) Diagram showing range of α values for which normal faults form (shaded area) and α values used in our models (α_1 defines the first-phase displacement direction, and α_2 defines the second-phase displacement direction). (b) Displacement and extension directions for models (E_1 is the first-phase extension direction, and E_2 is the second-phase extension direction).

3. Experimental observations

3.1. Large angle between extension directions

Model 1 has the maximum possible angular difference between displacement directions (90°) for which only normal faults form, and, therefore, the first- and second-phase extension directions are 45° apart (Fig. 2b). During the first phase of extension ($\alpha_1 = 45°$), numerous faults form in the deformation zone of the clay layer (Fig. 4a$_1$). Offset markers on the top surface of the clay layer and corrugations on the fault surfaces show that these faults are normal faults. Their strike is orthogonal to the

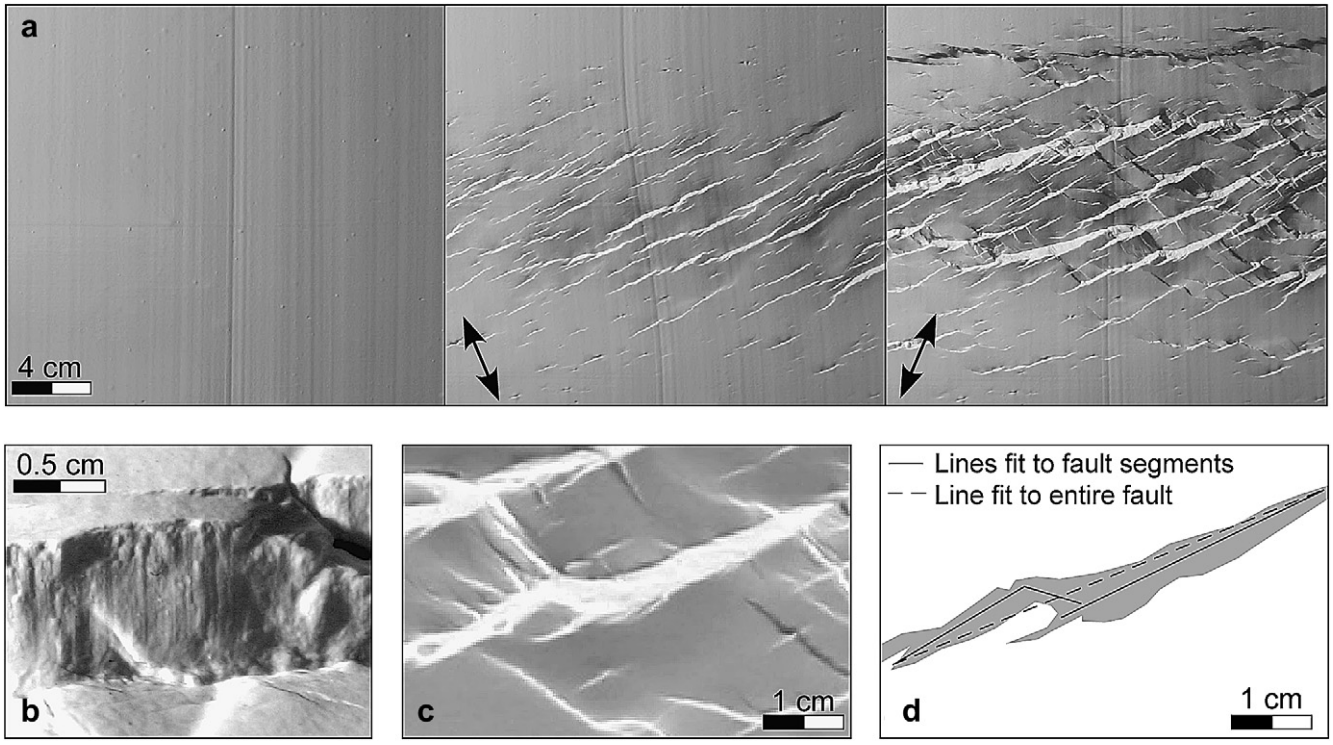

Fig. 3. Methods used in fault analysis. (a) Photographs of the top surface of the clay layer of Model 1 showing superficial linear markers at the beginning of the experiment (left), after the first phase of extension (middle), and after the second phase of extension (right). Offsets of markers indicate sense of slip on faults. Arrows indicate extension direction for each phase. (b) Photograph of slip-parallel corrugations on a fault surface. (c) Photograph of a segmented fault scarp (white on photograph). (d) Line drawing of segmented fault showing straight-line fit for each fault segment. Fitting lines to fault segments results in three distinct segments with three distinct orientations, whereas a tip-to-tip line yields one fault with one orientation.

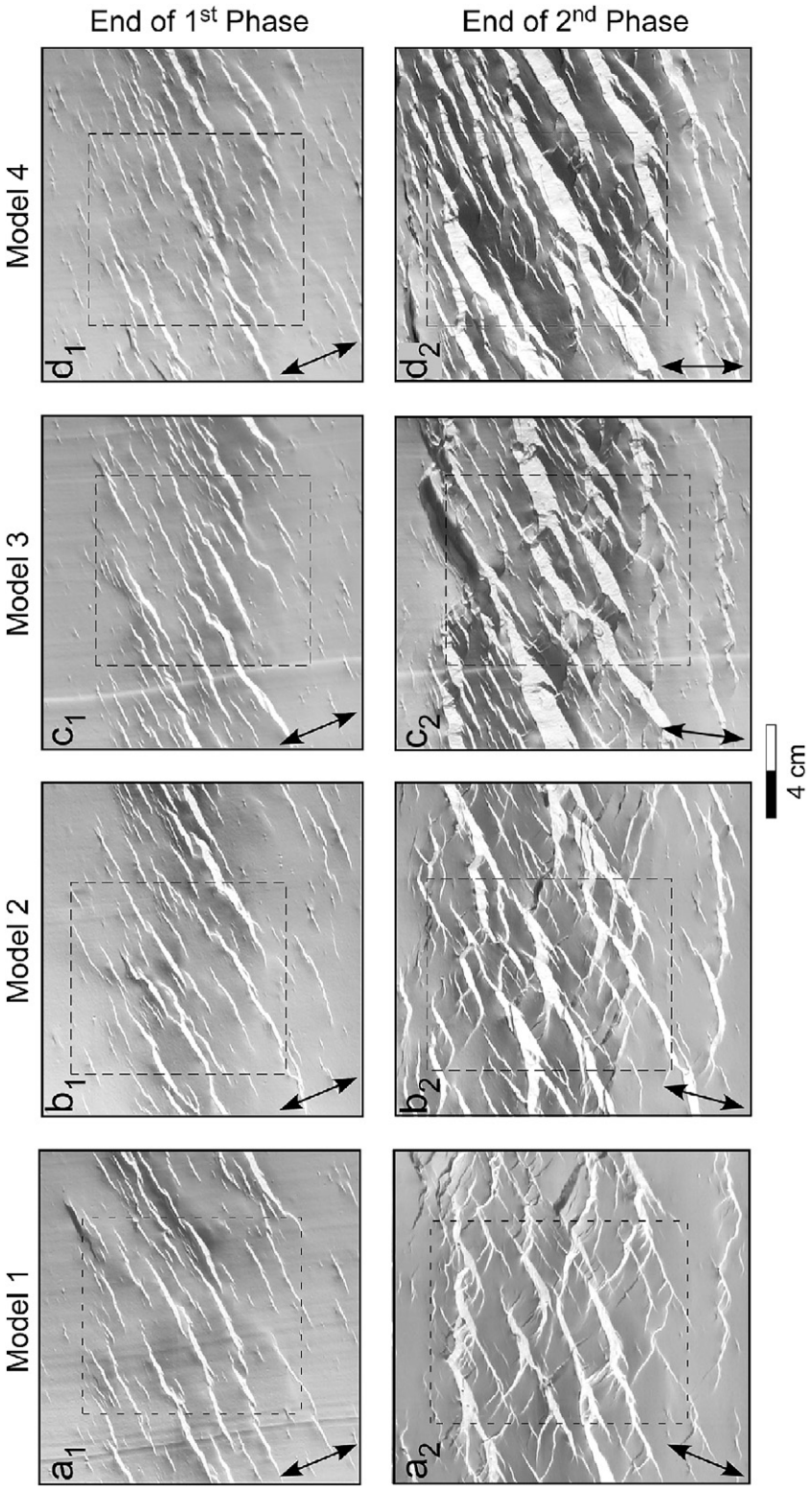

Fig. 4. Photographs of the top surface of the clay layer showing central region of the models after first and second phases of extension. Arrows indicate extension direction, and dashed box shows location of line drawings in Fig. 5. Fault scarps dipping toward the top of the page appear bright; fault scarps dipping toward the bottom of the page appear dark.

extension direction, and they dip ~60°. The fault pattern at the end of the first phase of Model 1 resembles those in other models of oblique extension with $\alpha = 45°$ (e.g., Withjack and Jamison, 1986; Tron and Brun, 1991; McClay and White, 1995; Clifton et al., 2000).

During the second phase of extension ($\alpha_2 = 135°$), many of the first-phase normal faults are reactivated with oblique slip (right-lateral and normal components) (Fig. 4a$_2$). The strike-slip component is significantly larger than the dip-slip component (Table 1). New normal faults also develop during the second phase of

Table 1
Fault-population statistics for second-phase deformation.

Model number	Angle between extension directions during 1st and 2nd phases	% of Fault population that form during 2nd phase	% of Dip-slip (normal) motion on reactivated faults during 2nd phase
1	45°	42	43
2	37.5°	33	50
3	30°	27	65
4	22.5°	12	70

extension (Figs. 4a$_2$, 5a$_2$). Most new normal faults initiate at first-phase faults and propagate away from them (Fig. 6). The strike of the new normal faults ranges from orthogonal to oblique to the second-phase extension direction, and many new faults change orientation during fault propagation. These faults are initially orthogonal to the pre-existing fault, and become approximately orthogonal to the second-phase extension direction as they propagate away from the pre-existing fault (Fig. 6). Where a new normal fault encounters a pre-existing fault, the new fault either cuts across the pre-existing fault or terminates against it (Fig. 7). In Model 1, more new normal faults cut across pre-existing faults (61%

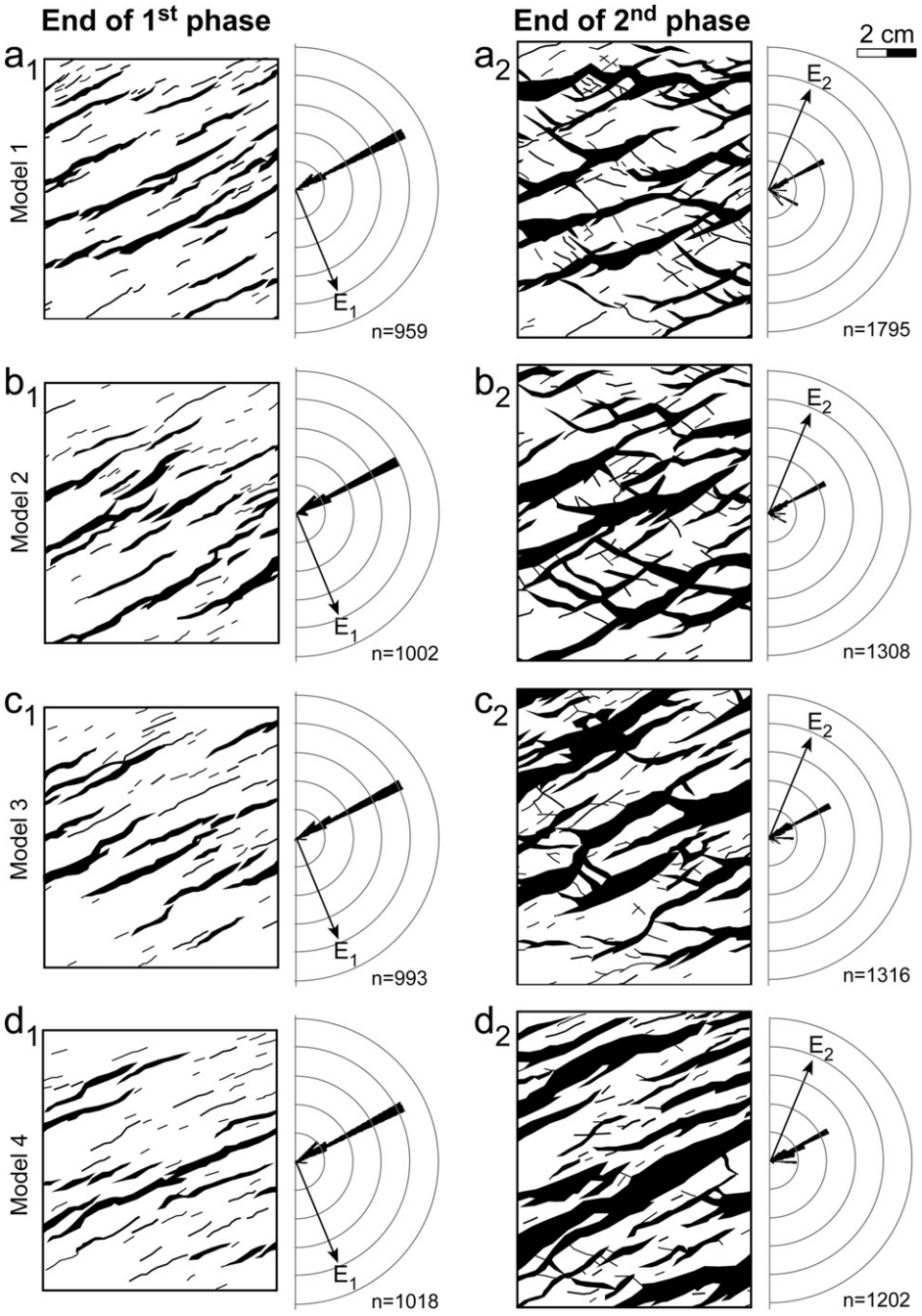

Fig. 5. Summary of modeling results. Line drawings of fault heaves are from the central region of the models (locations shown in Fig. 4). Rose diagrams show orientations of fault segments obtained using the method shown in Fig. 3. Arrows on rose diagrams show extension directions for each phase. Bin size for rose diagrams is 5°; the outside circle of each rose diagram equals 50% of the length-weighted fault segment population; n is the number of fault segments in a 40 cm by 12 cm area on the top surface of the clay layer from the central region of each model.

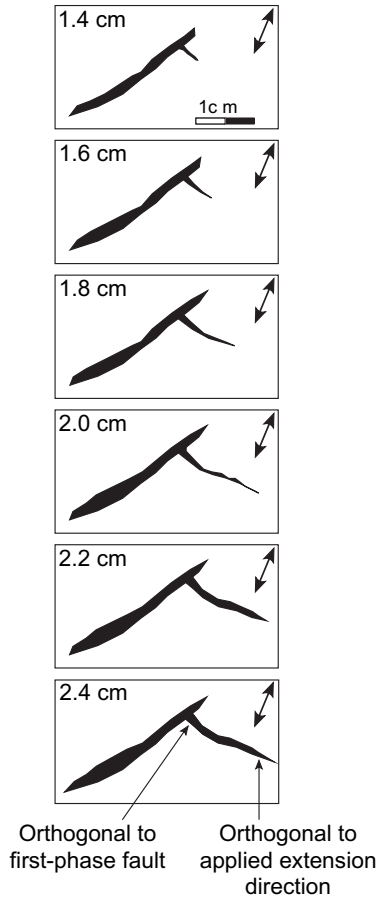

Fig. 6. Example of propagation of new normal faults during the second phase of extension for Model 1. Arrows show second-phase extension direction. Line drawings are from photographs of the top surface of the clay layer for progressively greater values of displacement of the movable sheet. As the new fault propagates outward from the pre-existing fault, its strike changes from orthogonal to the pre-existing fault to orthogonal to the extension direction.

of total fault interactions) than terminate against them (Fig. 7d). Generally, the new normal faults are significantly shorter than faults that form under identical conditions in the absence of a pre-existing fault fabric (Fig. 8b). In addition, the displacement on most of the new normal faults is greatest adjacent to the pre-existing fault and decreases outward (Fig. 8a). The interactions between the new faults and the first-phase faults create a complex fault pattern observable on both the top and bottom of the clay layer (Fig. 8c).

3.2. Moderate angles between extension directions

In Models 2 and 3 (which have 37.5° and 30° between the first- and second-phase extension directions, respectively), second-phase deformation is accommodated by reactivating the pre-existing normal faults and forming new normal faults (Fig. 4b_2, c_2). In both models, many of the first-phase faults are reactivated as oblique-slip faults with both normal and right-lateral strike-slip components. The magnitude of the normal component relative to the strike-slip component is larger in Models 2 and 3 than in Model 1 (Table 1), increasing as the angle between the directions of the first- and second-phase extension decreases. New normal faults form during the second phase of extension of both models (Fig. 5b_2, c_2), although fewer new fault segments develop in Models 2 and 3 than in Model 1 (Table 1). The strike of the new normal-fault segments ranges from orthogonal to oblique to the second-phase extension direction (Figs. 4, 5), and many new faults change orientation as they propagate. As in Model 1, new normal faults either cut across or terminate against the pre-existing faults. More new normal faults cut across pre-existing faults in Model 2 than in Model 3 (Fig. 7d).

3.3. Small angle between extension directions

In Model 4 (which has 22.5° between the first- and second-phase extension directions), few new normal faults form during the second phase of extension (Figs. 4d_2, 5d_2; Table 1). Instead, reactivation of the first-phase normal faults accommodates most

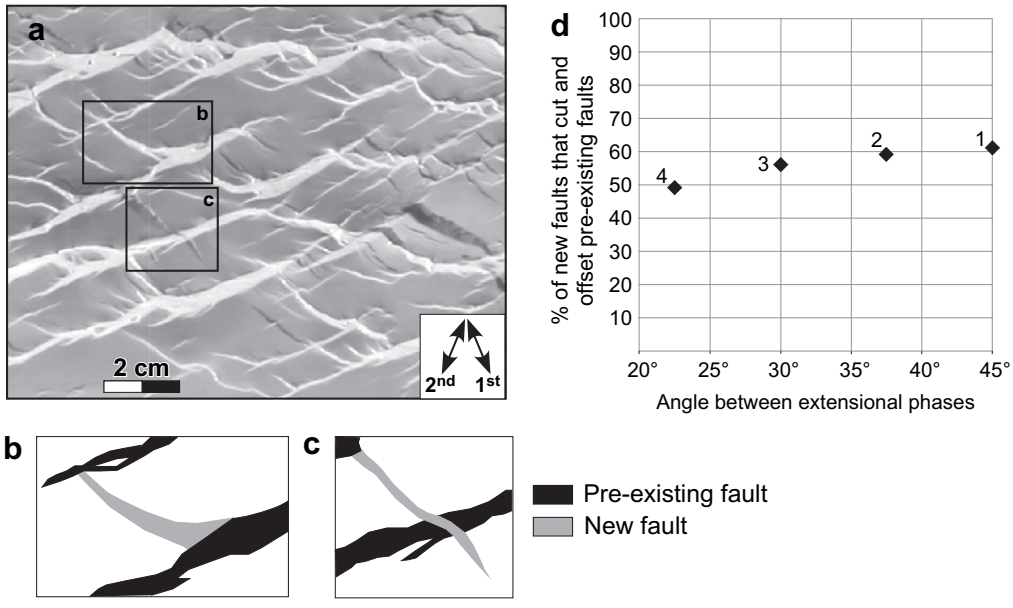

Fig. 7. Examples of fault interactions in the models. (a) Photograph of part of the top surface of the clay layer of Model 1. Fault scarps dipping toward the top of the page appear bright; fault scarps dipping toward the bottom of the page appear dark. (b) Line drawing showing a new normal fault terminating against a pre-existing fault. (c) Line drawing showing a new normal fault cutting and offsetting a pre-existing fault. (d) Graph showing the percentage of second-phase faults that cut and offset pre-existing faults (rather than terminate against pre-existing faults) for models. Numbers adjacent to the data points indicate the model designation.

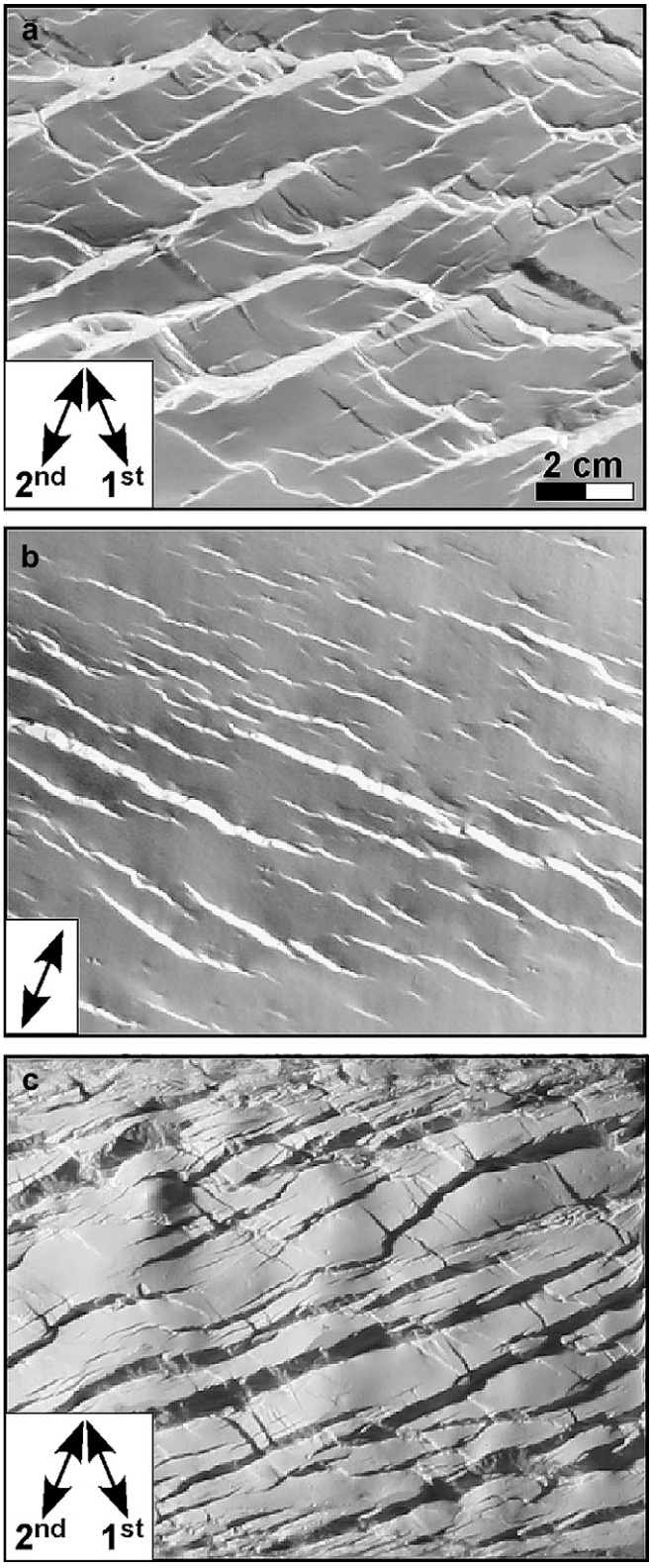

Fig. 8. (a) Photograph of the top surface of the clay layer of Model 1. (b) Photograph of the top surface of the clay layer of a different model subjected to the same second-phase extension as Model 1 but no first-phase extension. (c) Photograph of the bottom surface of the clay layer of a different model with the same boundary conditions as Model 1. Fault scarps dipping toward the top of the page appear bright; fault scarps dipping toward the bottom of the page appear dark. Fault dip directions appear reversed in (c) because it shows the bottom surface of the clay layer.

deformation (Fig. 4d$_2$). Motion on the reactivatied faults is mostly dip slip during the second phase, with a minor right-lateral strike-slip component (Table 1). Although corrugations are present on fault surfaces in all models, the two sets of corrugations associated with the two phases of extension are most prominent for this model (Fig. 9). New normal-fault segments constitute only a small part (12%) of the fault population in Model 4. The strike of these new normal-fault segments ranges from orthogonal to oblique to the second-phase extension direction. Although few new normal faults are present in this model, an almost equal percentage of the new normal faults cuts across or terminates against the first-phase faults (Fig. 7d).

4. Discussion

4.1. Summary of modeling results

The experimental models show that the normal faults that form during one episode of extension affect the faults that develop during subsequent episodes of extension. Specifically, our models show that the angle between the first and second phases of extension influences the sense of slip on reactivated first-phase faults and the abundance and orientation of second-phase normal faults. Both fault reactivation and new fault formation occur during the second phase of extension in our models (Figs. 4, 5). The reactivated faults have oblique slip, with the strike-slip component decreasing as the angle between the directions of the first- and second-phase extension decreases (Table 1). The number of new normal-fault segments also decreases as the angle between the first- and second-phase extension directions decreases (Fig. 5, Table 1). In Model 4, with an angle of 22.5° between the extension directions, most second-phase deformation is accommodated by fault reactivation with little formation of new normal faults (Figs. 4, 5).

Multiple fault populations are present in all of the models. After the first phase of extension, the strike of most fault segments is approximately orthogonal to the first-phase extension direction. Fault segments whose strike is oblique to the first-phase extension direction likely reflect fault linkage, and constitute only a small part

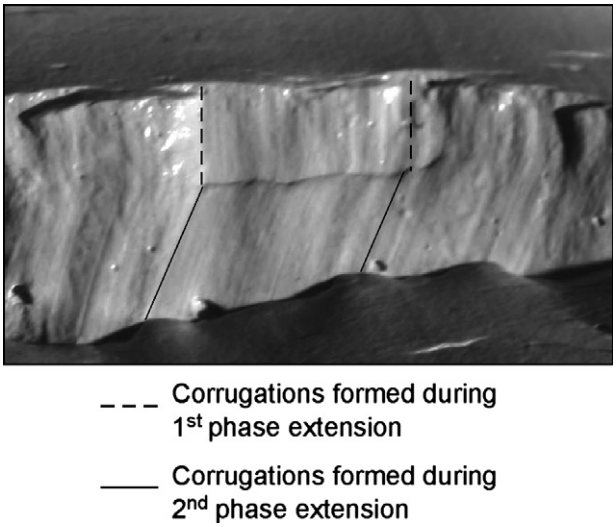

Fig. 9. Oblique-view photograph of fault surface in Model 4 showing two sets of corrugations. The corrugations parallel the slip direction during each phase of extension. This fault formed during the first phase of extension as a normal fault and was reactivated during the second phase as an oblique-slip fault (with normal and right-lateral strike-slip components).

(less than 5%) of the fault segment population (Fig. 5). After the second phase of extension, each model has normal-fault segments with strikes approximately orthogonal to the first-phase extension direction, approximately orthogonal to the second-phase extension direction, and oblique to both extension directions (Figs. 4, 5). The latter fault segments, with strikes oblique to both extension directions, likely reflect local perturbations in the stress/strain state near pre-existing faults (e.g., Homberg et al., 1997, 2004; Kattenhorn et al., 2000). As new normal faults propagate away from pre-existing faults, their strikes commonly change from orthogonal to the pre-existing faults to orthogonal to the applied extension direction (Fig. 6). However, many second-phase normal faults are confined by closely spaced, pre-existing faults, and never leave the perturbed stress/strain domain. This compartmentalization also limits the length of many second-phase normal faults.

4.2. Fault reactivation

The strength of most upper crustal rocks increases with depth, obeying a Mohr–Coulomb criterion of failure (e.g., Byerlee, 1978). According to this criterion,

$$\tau = C + \mu\sigma_n \quad (2)$$

where τ and σ_n are, respectively, the shear and normal stresses on a potential fault surface, C is the cohesive strength, and μ is the coefficient of internal friction. Once a fault surface forms, frictional-sliding controls failure according to the equation:

$$\tau = \mu_s \times \sigma_n \quad (3)$$

where τ and σ_n are the shear and normal stresses on a potential fault surface and μ_s is the coefficient of sliding friction along the fault plane. Pre-existing zones of weakness are likely to reactivate if the ratio of shear stress to normal stress on the surface of the pre-existing zone of weakness exceeds μ_s.

In all of our models, the orientation of σ_1 (the maximum principal stress) is vertical during both phases of extension. The orientations of σ_2 and σ_3 (the intermediate and minimum principal stresses), however, change between the first and second phases of extension. The minimum principal stress, σ_3, parallels the extension direction at the start of each extensional phase (ignoring any stress variations associated with the pre-existing faults). Thus, the first-phase normal faults, with dips of ~60° in the first-phase σ_1/σ_3 reference frame, have apparent dips between 51° (Model 1) and 58° (Model 4) in the second-phase σ_1/σ_3 reference frame (Fig. 10a, b). Although the exact value for the coefficient of sliding friction for clay is unknown, we assume that the frictional-sliding envelope parallels the Mohr–Coulomb failure envelope for intact clay (with $\mu \sim 0.6$ and $C \sim 50$ Pa) (Fig. 10c). Thus, the loss of cohesion on the fault surface is the only difference between the intact clay and the faulted clay after the first phase of extension. With this assumption, we expect faults with an apparent dip of about 45°

a

	Model 1	Model 2	Model 3	Model 4
Cross section parallel to σ_3 during 2nd phase (see b)	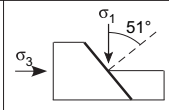	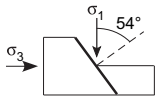	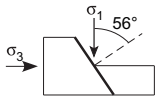	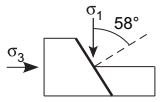
Angle between extension directions	45°	37.5°	30°	22.5°
Apparent dip of reactivated faults in σ_1/σ_3 reference frame during 2nd phase	51°	54°	56°	58°
θ^*	51°	54°	56°	58°
2θ	102°	108°	112°	116°

*θ is the angle between σ_1 and the normal to the fault plane

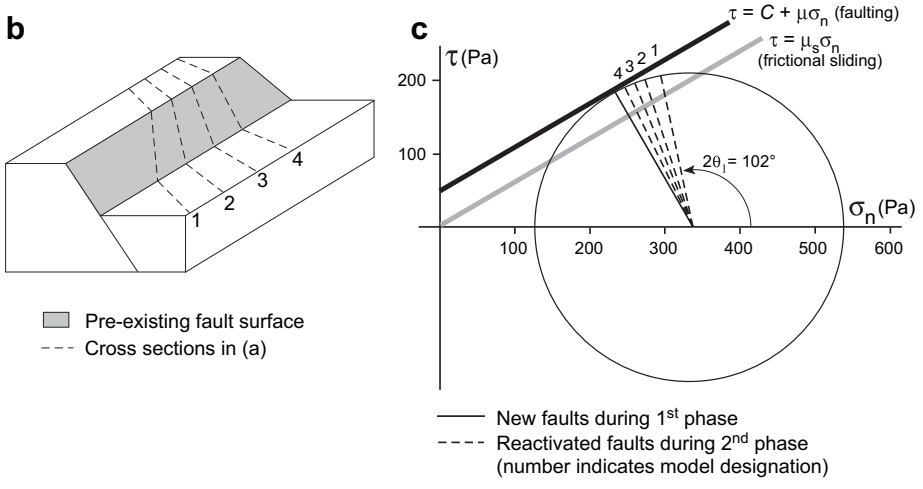

Fig. 10. (a) Stress regime for reactivated faults at the beginning of the second phase of extension for all models. (b) Block diagram showing orientation of cross sections shown in (a). (c) Mohr-circle diagram for stress state in the experimental models at the base of the 3.5-cm thick clay layer. Numbers 1–4 refer to the four different models. Black line shows the Mohr–Coulomb failure envelope for wet clay, and the grey line shows the assumed frictional-sliding failure envelope for wet clay. The two failure envelopes differ only by the value of cohesion.

and higher to be reactivated in our models (Fig. 10c). This agrees with the observations that all first-phase faults are reactivated as oblique-slip faults during the second phase of extension in our models.

4.3. Comparison to previous modeling studies

Bonini et al. (1997) and Keep and McClay (1997) simulated two non-coaxial phases of extension using a layer of dry sand overlying a basal layer of silicone polymer. Their models differ from our models in terms of the modeling material (dry sand vs. wet clay) and the width of the basal layer of silicone polymer (the entire base of the model vs. a narrow zone). Despite these differences, the modeling results are qualitatively similar. Their models show that faults that form during the first phase of extension influence the fault patterns that develop during the second phase of extension. Specifically, the reactivation of the first-phase faults during the second phase, the development of new second-phase faults, and the slip and attitude of the second-phase faults depend on the angle between the first- and second-phase extension directions. Reactivation is more likely when the angle is small, whereas new fault development is more likely when the angle is large. Our models support these conclusions. In addition, our models show that the angle between the first- and second-phase extension directions controls the relative components of dip slip and strike slip on the reactivated faults and the number of new faults that form during the second phase of extension. Furthermore, our models allow for the observation of small-scale features (such as the interaction between pre-existing faults and new faults) because faults are more numerous, have smaller displacements, and are more closely spaced in clay models than in sand models (e.g., Withjack et al., 2007). Our work, in combination with that of Bonini et al. (1997) and Keep and McClay (1997), illustrates that a pre-existing fault fabric substantially influences the fault patterns that develop during subsequent episodes of extension.

4.4. Natural examples of multi-phase extension

The fault interactions in our models are similar to those observed in nature. In the Terra Nova region of the Jeanne d'Arc rift basin of offshore Newfoundland, two main fault orientations (N–S and E–W) are present (e.g., Enachescu, 1987; Sinclair, 1995a, b) (Fig. 11a). Movement on N-striking normal faults occurred during the Late Jurassic through the early Early Cretaceous, whereas movement on E-striking normal faults occurred during the late Early Cretaceous (Sinclair, 1995a). Well and 3D seismic-reflection data show that some of the younger, E-striking normal faults cut and offset the older, N-striking normal faults, whereas others terminate against the older, N-striking normal faults (McIntyre et al., 2004) (Fig. 11b, c). The presence of both types of fault interactions in the Jeanne d'Arc rift basin matches our experimental observations that both types of fault interactions are likely to occur with multiple phases of non-coaxial extension. In addition, in many parts of the Jeanne d'Arc basin, displacement on the younger, E-striking normal faults is greatest adjacent to the older, N-striking normal faults (Fig. 11b). This displacement variation is common in our models where new faults initiate at pre-existing faults and propagate outward (Fig. 6). The modeling results suggest that the

Fig. 11. (a) Map of the Terra Nova region of the Jeanne d'Arc rift basin, offshore Newfoundland, showing faults offsetting the B marker (Early Cretaceous). Map modified from McIntyre et al. (2004). Insert shows location of the Jeanne d'Arc basin (box) relative to Newfoundland, Canada. (b) Younger, E-striking normal faults terminating against older, N-striking normal faults. (c) Younger, ESE-striking normal faults cutting and offsetting older, N-striking normal faults. Locations are shown in (a).

younger, E-striking normal faults initiated at and propagated outward from the older, N-striking normal faults.

Our modeling results also agree with natural observations of normal-fault reactivation. Studies of abyssal-hill normal faults in subduction zones (e.g., Masson, 1991; Moritera-Guitiérrez et al., 2003; Billen et al., 2007) show that the formation of new outer-slope normal faults (which form to accommodate bending-induced extension of subducting plates) depends on the orientation of the pre-existing abyssal-hill normal faults relative to the orientation of the trench axis. Abyssal-hill normal faults form at spreading centers to accommodate extension of newly forming crust, becoming permanent features of the oceanic crust (e.g., Rea, 1975; Kriner et al., 2006; and references therein). Moritera-Guitiérrez et al. (2003) and Billen et al. (2007) show that, if the angle between the trench axis and the strike of the pre-existing abyssal-hill faults is less than 25° (i.e., the angle between the first- and second-phase extension directions is less than 25°), then abyssal-hill normal faults are reactivated and no new normal faults form (Fig. 12b). If the angle between the trench axes and the strike of the abyssal-hill faults is greater than 25°, however, new outer-slope normal faults form that strike perpendicular to the bending-induced extension direction (i.e., parallel to the trench) (Fig. 12a). Observations from the Izu-Bonin Trench (Renard et al., 1987), the Middle American Trench (Masson, 1991), and the Aleutian Trench (Moritera-Guitiérrez et al., 2003) show that the pre-existing abyssal-hill normal faults may also be reactivated (in addition to new normal fault formation) if the angle between the trench and the abyssal-hill faults is greater than 25°. Our modeling results corroborate these observations: specifically, as the angle between the directions of the two phases of extension decreases from 30° to 22.5°, the strain accommodation changes from fault reactivation and new normal-fault formation (Model 3) to mainly fault reactivation (Model 4). This transition, however, is gradual, occurring between 30° and 22.5°. In addition, our models suggest that some of the reactivated abyssal-hill normal faults are likely to be oblique-slip faults.

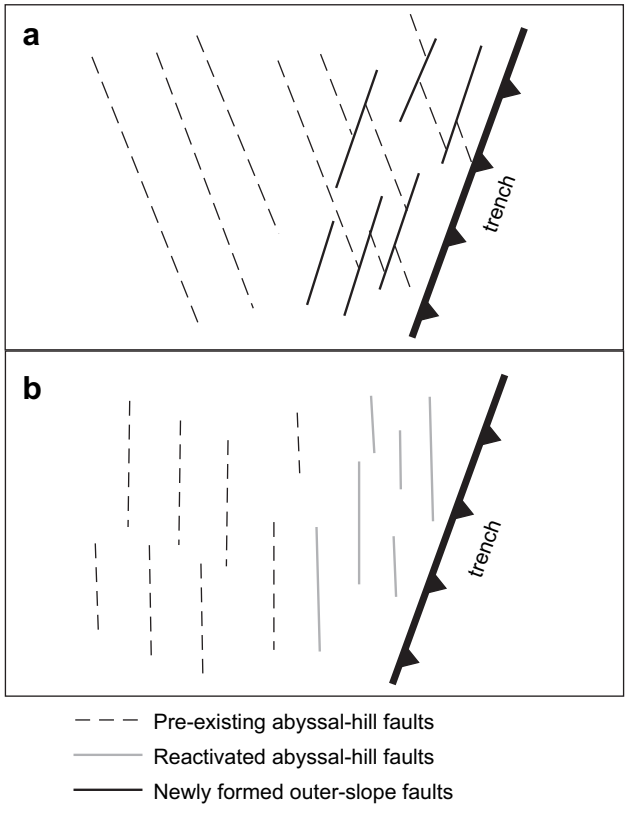

Fig. 12. Schematic map patterns showing development of outer-slope normal faults. (a) New outer-slope normal faults form if the angle between the trench axis and the strike of pre-existing abyssal-hill normal faults is greater than 25°. (b) Abyssal-hill normal faults reactivate and no new outer-slope normal faults form if the angle between the trench axis and the strike of the abyssal-hill normal faults is less than 25°. Modified from Billen et al. (2007).

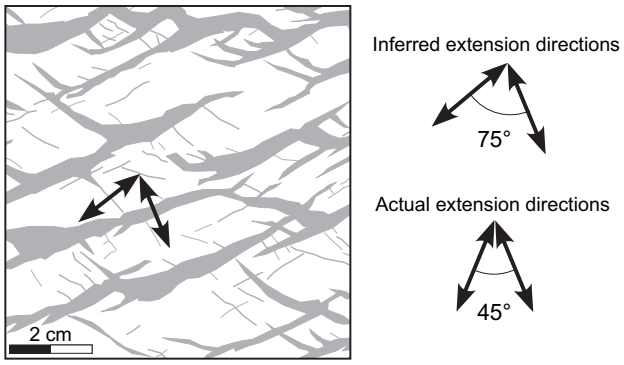

Fig. 13. Line drawing of the top surface of the clay layer of Model 1 after both phases of extension (location shown in Fig. 4). Arrows indicate inferred extension directions determined by assuming that extension is orthogonal to the strike of the normal faults. The angle between the *inferred* extension directions is 75°, although the *actual* angle between the extension directions is 45°.

4.5. Predicting strain state from fault orientations

Fault orientations are commonly used to estimate the paleo-strain states in extensional provinces by assuming that the strike of the normal faults is perpendicular to the direction of the maximum horizontal extension (and presumably the direction of σ_3) as predicted by Anderson (1951). Our modeling results illustrate that, in areas with multiple extensional episodes, fault orientations are influenced by local perturbations in the stress/strain state associated with pre-existing faults and, thus, are not reliable paleo-strain indicators (Fig. 13).

In addition, our modeling results suggest that fault interactions do not necessarily provide information about the order of extensional phases. For example, the second-phase normal faults in our models either cut the first-phase normal faults or terminate against them. Second-phase faults that terminate against first-phase faults may be misinterpreted as coeval releasing faults (as defined by Destro, 1995), or they may appear to be cut by the first-phase faults and erroneously considered to be older. Fault orientations, fault slip, and timing of fault activity (based on the presence or absence of growth beds) are all necessary to determine the paleo-strain state. Without this information, the directions and relative timing of extension determined from fault interactions represent only one of many possible deformational histories.

5. Conclusions

We have used scaled experimental models to study how a pre-existing fault fabric affects subsequent deformation during multiple phases of extension. The models indicate that pre-existing faults are reactivated for a range of second-phase extension directions. In addition, pre-existing faults influence the fault patterns that form during subsequent extensional episodes by controlling new fault orientations, lengths, and locations.

- The angle between the strike of the pre-existing normal faults and the second-phase extension direction controls the sense of slip on the reactivated faults, with the component of dip slip relative to strike slip decreasing as the angle between the first- and second-phase extension directions increases.
- New normal faults form during the second phase of extension in all models. These faults are generally shorter than faults that form in models with no pre-existing fault fabric. The number of new fault segments varies between models, with more new fault segments forming as the angle between the first- and second-phase extension directions increases.
- The orientations of new normal-fault segments are both orthogonal and oblique to the second-phase extension direction. New normal faults with strikes oblique to the second-phase extension direction likely reflect local perturbations in the stress/strain state near pre-existing faults.
- New normal faults commonly initiate at pre-existing normal faults and propagate outward. Displacement on these new normal faults is greatest adjacent to the pre-existing faults. Where new normal faults encounter pre-existing faults, the new faults either cut across the pre-existing faults or terminate against them.
- Fault interactions and fault reactivations in the models are similar to those observed in nature, including the Jeanne d'Arc rift basin of offshore Newfoundland and at outer highs near subduction zones.
- Interpretations of extensional histories based solely on fault orientations and fault interactions represent only one of many possible deformation histories. Additional information, such as fault slip and the timing of fault activity (i.e., the presence or absence of growth beds), is necessary to constrain the paleo-strain state.

Acknowledgments

We thank our colleagues Michael Durcanin, Iain Sinclair, and Judith McIntyre for valuable discussions and insights about modeling and fault interactions and Hemal Vora for his assistance in the laboratory. We also thank Marco Bonini, Chris Jackson, and Bruno Vendeville for their detailed and helpful reviews of the manuscript. We gratefully acknowledge the support of the Structural Modeling Laboratory at Rutgers University by the National Science Foundation (EAR-0838462 and EAR-0408878), Husky Energy Inc., and Petrobras S.A.

References

Anderson, E.M., 1951. The Dynamics of Faulting and Dyke Formation with Applications to Britain. Oliver & Boyd, Edinburgh.

Badley, M.E., Price, J.D., Dahl, C.R., Agdestein, T., 1988. The structural evolution of the northern Viking Graben and its bearing upon extensional models of basin formation. Journal of the Geological Society, London 145, 455–472.

Bartholomew, I.D., Peters, J.M., Powell, C.M., 1993. Regional structural evolution of the North Sea: oblique slip and the reactivation of basement lineaments. In: Parker, J.R. (Ed.), Petroleum Geology of Northwest Europe: Proceedings of the Fourth Conference. The Geological Society, London, pp. 1109–1122.

Bellahsen, N., Daniel, J.M., Bollinger, L., Burov, E., 2003. Influence of viscous layers on the growth of normal faults: insights from experimental and numerical models. Journal of Structural Geology 25, 1471–1485.

Billen, M., Cowgill, E., Buer, E., 2007. Determination of fault friction from reactivation of abyssal-hill faults in subduction zones. Geology 35, 819–822.

Bonini, M., Souriot, T., Boccaletti, M., Brun, J.P., 1997. Successive orthogonal and oblique extension episodes in a rift zone: laboratory experiments with application to the Ethiopian Rift. Tectonics 16, 347–362.

Brace, W.F., Kohlstedt, D.L., 1980. Limits on lithospheric stress imposed by laboratory experiments. Journal of Geophysical Research 85, 6248–6252.

Byerlee, J., 1978. Friction of rocks. Pure and Applied Geophysics 116, 615–626.

Clifton, A.E., Schlische, R.W., Withjack, M.O., Ackermann, R.V., 2000. Influence of rift obliquity on fault-population systematics: results of clay modeling experiments. Journal of Structural Geology 22, 1491–1509.

Destro, N., 1995. Release fault: a variety of cross fault in linked extensional fault systems, in the Sergipe-Alagoas Basin, NE Brazil. Journal of Structural Geology 17, 615–629.

Eisenstadt, G., Sims, D., 2005. Evaluating sand and clay models: do rheological differences matter? Journal of Structural Geology 27, 1399–1412.

Enachescu, M.E., 1987. Tectonic and structural framework of the northeast Newfoundland continental margin. In: Beaumont, C., Tankard, A.J. (Eds.), Sedimentary Basins and Basin-Forming Mechanisms. Canadian Society of Petroleum Geologists Memoir 12, 117–146.

Færseth, R.B., 1996. Interaction of Permo-Triassic and Jurassic extensional fault-blocks during the development of the northern North Sea. Journal of the Geological Society, London 153, 931–944.

Granger, A.B., 2006. Influence of basal boundary conditions on normal-fault systems in scaled physical models. Masters thesis, Rutgers University.

Granger, A.B., Withjack, M.O., Schlische, R.W., 2006. Undulations on normal-fault surfaces: insights into fault growth using scaled physical models of extension. Geological Society of America Abstracts with Program 38, p. 480.

Granger, A.B., Withjack, M.O., Schlische, R.W., September 2008. Fault surface corrugations: insights from scaled experimental models of extension. In: "Fault Zones: Structure, Geomechanics, and Fluid Flow" Conference, Abstracts Volume. Geological Society of London. 38.

Handin, 1966. Strength and ductility. In: Clark, S.P. (Ed.), Handbook of Physical Constants, 97. Geological Society of America Memoir, pp. 233–289.

Homberg, C., Hu, J.C., Angelier, J., Bergerat, F., Lacombe, O., 1997. Characterization of stress perturbations near major fault zones: insights from 2D distinct-element numerical modelling and field studies (Jura mountains). Journal of Structural Geology 19, 703–718.

Homberg, C., Angelier, J., Bergerat, F., Lacombe, O., 2004. Using stress deflections to identify slip events in fault systems. Earth and Planetary Science Letters 217, 409–424.

Hubbert, M.K., 1937. Theory of scale models as applied to the study of geological structures. Geological Society of America Bulletin 48, 1459–1519.

Kattenhorn, S.A., Aydin, A., Pollard, D.D., 2000. Joints at high angles to normal fault strike: an explanation using 3-D numerical models of fault-perturbed stress fields. Journal of Structural Geology 22, 1–23.

Keep, M., McClay, K.R., 1997. Analogue modeling of multiphase rift systems. Tectonophysics 273, 239–270.

Kriner, K.K., Pockalny, R.A., Larson, R.L., 2006. Bathymetric gradients of lineated abyssal hills: inferring seafloor spreading vectors and a new model for hills formed at ultra-fast rates. Earth and Planetary Science Letters 242, 98–110.

Masson, D.G., 1991. Fault patterns at outer trench walls. Marine Geophysical Researches 13, 209–225.

McIntyre, J., DeSilva, N., Thompson, T., 2004. Mapping of key geological markers in the Jeanne d'Arc basin based on 3-D seismic. Canadian Society of Petroleum Geologists Annual Meeting.

McClay, K.R., White, M.J., 1995. Analogue modeling of orthogonal and oblique rifting. Marine and Petroleum Geology 12, 137–151.

Moritera-Guitiérrez, C.A., Scholl, D.W., Carlso, R.L., 2003. Fault trends on the seaward slope of the Aleutian Trench: implications for a laterally changing stress field tied to a westward increase in oblique convergence. Journal of Geophysical Research 108. doi:10.1029/2001JB001433.

Morley, C.K., Gabdi, S., Seusutthiya, K., 2007. Fault superimposition and linkage resulting from stress changes during rifting: examples from 3D seismic data, Phitsanulok Basin, Thailand. Journal of Structural Geology 29, 646–663.

Morley, C.K., Harayana, C., Phoosongsee, W., Pongwapee, S., Kornsawan, A., Wonganan, N., 2004. Activation of rift oblique and rift parallel pre-existing fabrics during extension and their effect on deformation style: examples from the rifts of Thailand. Journal of Structural Geology 26, 1803–1829.

Nalpas, T., Brun, J.P., 1993. Salt flow and diapirism related to extension at crustal scale. Tectonophysics 228, 349–362.

Rea, D.K., 1975. Model for the formation of topographic features of the East Pacific Rise Crest. Geology 3, 77–80.

Renard, V., Nakamure, K., Angelier, J., Azema, J., Bourgois, J., Deplus, C., Fujioka, K., Hamano, Y., Huchon, P., Kinoshita, H., Labaume, P., Ogawa, Y., Seno, T., Takeuchi, A., Tanahashi, M., Uchiyama, A., Vigneresse, J.L., 1987. Trench triple junction off Central Japan – preliminary results of the French–Japanese 1984 Kaiko cruise, Leg 2. Earth and Planetary Science Letters 83, 243–256.

Schellart, W.P., 2000. Shear test results for cohesion and friction coefficients for different granular materials: scaling implications for their usage in analogue modeling. Tectonophysics 324, 1–16.

Sinclair, I.K., 1995a. Transpressional inversion due to episodic rotation of extensional stresses in Jeanne d'Arc Basin, offshore Newfoundland. In: Buchanan, J.G., Buchanan, P.G. (Eds.), Basin Inversion. Geological Society Special Publication 88, pp. 249–271.

Sinclair, I.K., 1995b. Sequence stratigraphic response to Aptian–Albian rifting in conjugate margin basins: a comparison of the Jeanne d'Arc Basin, offshore Newfoundland, and the Porcupine Basin, offshore Ireland. In: Scrutton, R.A., Stoker, M.S., Shimmield, G.B., Tudhope, A.W. (Eds.), The Tectonics, Sedimentation, and Palaeoceanography of the North Atlantic Region. Geological Society Special Publication 90, pp. 29–49.

Sinclair, I.K., Withjack, M.O., 2008. Mid to Late Cretaceous structural and sedimentary architecture at the Terra Nova oilfield, offshore Newfoundland – implications for tectonic history of the North Atlantic. In: Brown, D.E. (Ed.), Central Atlantic Conjugate Margins. Dalhousie University, Halifax, Nova Scotia, pp. 125–141.

Strecker, M.R., Blisniuk, P.M., Eisbacher, G.H., 1990. Rotation of extension direction in the central Kenyan Rift. Geology 18, 299–302.
Tankard, A.J., Welsink, H.J., 1987. Extensional tectonics and stratigraphy of Hibernia oil field, Grand Banks, Newfoundland. AAPG Bulletin 71, 1210–1232.
Tron, V., Brun, J.P., 1991. Experiments on oblique rifting in brittle-ductile systems. Tectonophysics 188, 71–84.
Weijermars, R., 1986. Flow behaviour and physical chemistry of bouncing putties and related polymers in view of tectonic laboratory applications. Tectonophysics 124, 325–358.
Weijermars, R., Jackson, M.P.A., Vendeville, B.C., 1993. Rheological and tectonic modeling of salt provinces. Tectonophysics 217, 143–174.
Withjack, M.O., Callaway, J.S., 2000. Active normal faulting beneath a salt layer: An experimental study of deformation in the cover sequence. AAPG Bulletin 84, 627–652.
Withjack, M.O., Jamison, W.R., 1986. Deformation produced by oblique rifting. Tectonophysics 126, 99–124.
Withjack, M.O., Schlische, R.W., 2006. Geometric and experimental models of extensional fault-bend folds. In: Buiter, S.J.H., Schreurs, G. (Eds.), Analogue and Numerical Modelling of Crustal-Scale Processes. Geological Society (London) Special Publication 253, pp. 285–305.
Withjack, M.O., Schlische, R.W., Henza, A.A., 2007. Scaled experimental models of extension: dry sand vs. wet clay. Houston Geological Survey Bulletin 49 (8), 31–49.